HHS Public Access

Author manuscript

J Cell Physiol. Author manuscript; available in PMC 2021 November 01.

Published in final edited form as:

J Cell Physiol. 2020 November ; 235(11): 8520–8532. doi:10.1002/jcp.29696.

NUCLEAR FACTOR OF ACTIVATED T CELLS 1 AND 2 ARE REQUIRED FOR VERTEBRAL HOMEOSTASIS

Ernesto Canalis[*,1,2,3], **Lauren Schilling**[3], **Tabitha Eller**[3], **Jungeun Yu**[1,3]

[1]Department of Orthopaedic Surgery, UConn Health, Farmington, CT 06030

[2]Department of Medicine, UConn Health, Farmington, CT 06030

[3]UConn Musculoskeletal Institute, UConn Health, Farmington, CT 06030

Abstract

The present study defines the function of NFATC1 and NFATC2 in osteoblast function *in vivo* and *in vitro*. *Nfatc1*$^{loxP/loxP}$, *Nfatc2*$^{loxP/loxP}$ and *Nfatc1*$^{loxP/loxP}$;*Nfatc2*$^{loxP/loxP}$ conditional mice were mated with *BGLAP-Cre* transgenics to inactivate *Nfatc1* and *Nfatc2* singly and in combination in osteoblasts. Microcomputed tomography demonstrated that male and female conditionally inactivated *Nfatc1, Nfatc2* and dual *Nfatc1;Nfatc2* mice had osteopenia at Lumbar 3 (L3) sites when compared to littermate controls. However, the *Nfatc1* and *Nfatc2* inactivation singly and in combination in *Bglap*-expressing osteoblasts did not result in an appreciable phenotype at femoral sites. Bone histomorphometry of L3 confirmed the osteopenic phenotype and demonstrated that *Nfatc1;Nfatc2* inactivated male mice had a significant decrease in osteoblast number and in osteoblast surface and osteoid surface The dual downregulation of *Nfatc1* and *Nfatc2* in bone marrow stromal cells caused a decrease in *Alpl* and *Bglap* expression, confirming a role of these transcription factors in osteoblast function.

In conclusion, our studies reveal that NFATc1 and NFATc2 are necessary for optimal vertebral, but not femoral, bone homeostasis *in vivo* and osteoblast differentiation *in vitro*.

Keywords

NFATc2; bone formation; bone remodeling; osteoblasts

INTRODUCTION

The fate and the function of cells of the osteoblast lineage becomes defined by transcription factors acting in concert so that cellular maturity is reached and the cells acquire the function and properties of osteoblasts (Bianco & Gehron, 2000). Nuclear factor of activated T cells (NFAT) are intracellular proteins (NFATc1 to c4 and NFAT5) critical for a normal immune response and known to regulate cell differentiation in various lineages (Crabtree & Olson,

[*]Address correspondence to: Ernesto Canalis, M.D., Departments of Orthopaedic Surgery and Medicine, UConn Health, Farmington, CT 06030-4037, Telephone: (860) 679-7978; Fax: (860) 679-1474; canalis@uchc.edu.

Disclosures: The authors declare no conflicts of interest with the contents of this article. The data that support the findings of this study are available from the corresponding author upon reasonable request.

2002; Graef, Chen, & Crabtree, 2001; Sitara & Aliprantis, 2010). Therefore, NFATs regulate cellular events in immune and non-immune cells including cells residing in the bone environment.

NFATc1, c2, c3 and c4 are synthesized by skeletal cells, and NFATc1 has been recognized as one essential factor in the differentiation of myeloid cells toward mature osteoclasts (Aliprantis et al., 2008; Ikeda et al., 2006; Ikeda et al., 2004; Ishida et al., 2002; Matsuo et al., 2004; Takayanagi et al., 2002). Indeed, *Nfatc1* deficient mice are osteopetrotic due to a lack of bone resorbing cells (Aliprantis et al., 2008). NFATc2 plays a less apparent role in the differentiation and function of osteoclasts (Ikeda et al., 2006; Ranger et al., 1998). The expression of a constitutively active form of NFATc2 (caNFATc2) directed by the *Acp5* gene induces osteoclast formation and as a consequence promotes the resorption of bone (Ikeda et al., 2006). The deletion *Nfatc2* in the myeloid lineage results in a decrease in osteoclastogenesis *in vitro*, but the deletion of *Nfatc2* in myeloid cells does not result in skeletal manifestations *in vivo* and results from the global downregulation of *Nfatc2* have been conflicting (Asagiri et al., 2005; Bauer et al., 2011; Yu, Zanotti, Schilling, & Canalis, 2018).

The role of NFATs in the differentiation of osteoblasts and the formation of bone is not as clearly established as their function in osteoclastogenesis and bone resorption. *In vitro*, expression of either caNFATc1 or caNFATc2 inhibits osteoblastogenesis (Zanotti, Smerdel-Ramoya, & Canalis, 2011, 2013). Accordingly, production of caNFATc2 in *Col1a1*-expressing osteoblasts causes osteopenia because of decreased osteoblastogenesis (Zanotti & Canalis, 2015). NFATs are activated following the dephosphorylation of serine residues by calcineurin, a phosphatase, and as a consequence NFATs translocate from the cytoplasm to the nucleus (Chow, Hou, & Bendeck, 2008; Hogan, Chen, Nardone, & Rao, 2003; Okamura et al., 2000). Studies in mouse models of calcineurin activation or inactivation in osteoblasts yielded conflicting outcomes so that the function of NFATs in osteoblast function and bone formation is not clearly defined (Sun et al., 2005; Yeo et al., 2007).

Murine models of *Nfatc1* and *Nfatc2* inactivation have demonstrated an inhibitory function of NFATs on chondrogenesis, and NFATs restrict osteochondroma formation both indicative of a role in chondrogenic cells (Ge et al., 2016; Ranger et al., 2000). However, *in vivo* models of *Nfatc1* and *Nfatc2* inactivation have not been used to establish the function of these transcription regulators in osteoblasts.

The purpose of the work being presented is to establish the contributions of NFATc1 and NFATc2, singly and in combination, to the differentiation and function of osteoblasts. To this end, we obtained $Nfatc1^{loxP/loxP}$ and utilized $Nfatc2^{loxP/loxP}$ conditional mice recently created by our group (Aliprantis et al., 2008; Yu et al., 2018). *Nfatc1* and *Nfatc2* were downregulated by Cre recombination under the control of *BGLAP*, which encodes osteocalcin, using a transgenic model previously reported to inactivate calcineurin in osteoblasts (Yeo et al., 2007; Zhang et al., 2002). The skeletal phenotype of conditional *Nfatc1*, *Nfatc2* and dual *Nfatc1;Nfatc2* null mice was examined by microcomputed tomography (μCT) of vertebral and femoral bones. In addition, the consequences of the *Nfatc1* and *Nfatc2* inactivation on osteoblast differentiation were determined *in vitro*.

MATERIALS AND METHODS

Nfatc1 and Nfatc2 Conditional and Cre-driver Mice

Nfatc2 conditional mice created in this laboratory were described previously and were backcrossed into a C57BL/6J background for ≥7 generations following the removal of the PGK-neo selection cassette as described (Yu et al., 2018). In this model, exon 2, which codes for the regulatory domain of NFATc2, is flanked by loxP sites and is removed by Cre recombination. This leads to a frame shift and the creation of a termination codon in exon 3, and the mature protein is devoid of regulatory and DNA binding domains (Okamura et al., 2000). *Nfatc1* conditional mice, where loxP sites flank exon 3 of *Nfatc1*, were obtained from L. Glimcher and studied in a C57BL/6J background (Boston, MA) (Aliprantis et al., 2008).

BGLAP-Cre mice in a C57BL/6J background (Jackson Laboratory, Stock 019509), were used to inactivate *Nfatc1*, *Nfatc2* or both in mature osteoblasts (Zhang et al., 2002). To inactivate *Nfatc1*, *Nfatc2* or both, mice homozygous for $Nfatc1^{loxP/loxP}$, $Nfatc2^{loxP/loxP}$ or $Nfatc1^{loxP/loxP}$;$Nfatc2^{loxP/loxP}$ alleles and heterozygous for the *BGLAP-Cre* allele were bred with $Nfatc1^{loxP/loxP}$, $Nfatc2^{loxP/loxP}$ or $Nfatc1^{loxP/loxP}$;$Nfatc2^{loxP/loxP}$ mice, respectively. As a result, *BGLAP-Cre*;$Nfatc1^{\Delta/\Delta}$, *BGLAP-Cre*;$Nfatc2^{\Delta/\Delta}$ and *BGLAP-Cre*;$Nfatc1^{\Delta/\Delta}$;$Nfatc2^{\Delta/\Delta}$ and $Nfatc1^{loxP/loxP}$, $Nfatc2^{loxP/loxP}$ and $Nfatc1^{loxP/loxP}$;$Nfatc2^{loxP/loxP}$ control littermates were created.

Conditionally deleted mice were compared to littermate controls of the same sex and genetic composition. Genotyping of *BGLAP-Cre*, $Nfatc1^{loxP}$ and $Nfatc2^{loxP}$ alleles was performed by polymerase chain reaction (PCR) in DNA extracts obtained from mouse tails (Table 1). Cre-dependent recombination of *loxP* flanked sequences was documented by PCR in DNA extracted from tibiae or calvariae. All animal experiments were approved by the Animal Care and Use Committee of either Saint Francis Hospital and Medical Center or the University of Connecticut Health Center.

Microcomputed Tomography

Femoral and vertebral (L3) microarchitecture was defined using a μCT40 microcomputed tomography instrument (Scanco Medical AG, Basserdorf, Switzerland). Calibration was performed weekly using a manufacturer-provided phantom (Bouxsein et al., 2010; Glatt, Canalis, Stadmeyer, & Bouxsein, 2007). Femurs and vertebrae were placed in 70% ethanol for scanning, which was conducted at an energy level of 55 peak kV, intensity of 145 μA and integration time of 200 ms. Evaluation of skeletal microarchitecture was started ~1.0 mm from the cranial side of the L3 vertebral body, or 1.0 mm proximal from the condyles of the distal femur. A total of 160 consecutive 6 μm thick slices were acquired at an isotropic voxel dimension of 261μm^3 and selected for analysis. Contours were drawn manually every 10 slices a few voxels away from the endocortical boundary to define the region of analysis. The remaining slice contours were iterated automatically. Cancellous bone was assessed for bone volume fractions (bone volume/total volume, BVTV), trabecular separation (Tb.Sp), number (Tb.N) and thickness (Tb.Th), connectivity density (Conn.D), structure model index (SMI) and material density using a Gaussian filter ($\sigma = 0.8$) (Bouxsein et al., 2010; Glatt et al., 2007). For femoral bone, user-defined thresholds were used and vertebral L3 were

analyzed using 290 pernil equivalent to 465 mg hydroxyapatite/cm^3 thresholds. Cortical bone was analyzed in femurs, where contours were iterated across 100 slices along the cortical shell of the femoral mid-shaft, excluding the marrow cavity. Analyses of BV/TV, cortical thickness, periosteal perimeter, endosteal perimeter, total cross-sectional and cortical bone area were performed using a Gaussian filter ($\sigma = 0.8$) and user-defined thresholds. The terminology and units used are in accordance with guidelines published in the Journal of Bone and Mineral Research (Bouxsein et al., 2010).

Bone Histomorphometry

Bone histomorphometric analysis was performed in 4 month old mice previously injected with calcein 20 mg/kg and demeclocycline 50 mg/kg at a 7 day interval and sacrificed 2 days after demeclocycline administration, as previously reported (Canalis, Schilling, Yee, Lee, & Zanotti, 2016; Canalis, Yu, Schilling, Yee, & Zanotti, 2018). L3 vertebrae were placed in 70% ethanol for fixation prior to being embedded in methyl methacrylate. Vertebral bodies were sectioned at a thickness of 5 μm along the coronal plane on a Microm microtome (Richards-Allan Scientific, Kalamazoo, MI). Static and dynamic parameters of bone morphometry were measured in a defined area at a magnification of 100x using OsteoMeasure software (Osteometrics, Atlanta, GA). Trabecular bone area, number and thickness, osteoblast, osteocyte and osteoclast number, osteoid and eroded surface were measured in toluidine blue (0.1%) stained sections. Mineralizing surface per bone surface and mineral apposition rate were measured on unstained sections visualized under UV light and values used to calculate bone formation rate. Terminology and units used for bone histomorphometry are those recommended by the Histomorphometry Nomenclature Committee of the American Society for Bone and Mineral Research (Dempster et al., 2013; Parfitt et al., 1987).

Bone Marrow Stromal Cell Cultures

Bone marrow stromal cells were obtained from femurs and tibiae dissected from 6 to 8 week old *Nfatc1*$^{loxP/loxP}$;*Nfatc2*$^{loxP/loxP}$ mice. Bone marrow cells were isolated by centrifugation following the removal of the epiphyseal ends and recovered in α-minimum essential medium (α-MEM, Life Technologies, Grand Island, NY). Cells were seeded at a density of 1.25×10^6 cells/cm^2 in α-MEM supplemented with 15% heat-inactivated fetal bovine serum (FBS) and grown in an incubator in an atmosphere of 5% CO_2 at 37°C. Cells in suspension were removed by replacing the culture medium 48 h after seeding and adherent cells were considered bone marrow stromal cells (Bianco & Gehron, 2000). Four to 5 days later adherent cells were digested with trypsin, replated and exposed to α-MEM containing 10% FBS, and grown to ~70% confluence, transferred to α-MEM supplemented with 2% FBS for 1 h and exposed overnight to 100 multiplicity of infection of replication defective recombinant adenoviruses. Adenoviral vector systems expressing Cre, to excise loxP flanked sequences (Ad-CMV-Cre), or green fluorescent protein (control, Ad-CMV-GFP, Vector Biolabs) both under the control of the cytomegalovirus (CMV) promoter were used. Cells were allowed to recover for 24 to 48 h and cultured in α-MEM 10% FBS to confluence and then in α-MEM supplemented with 10% FBS, 100 μg/ml ascorbic acid and 5 mM β-glycerophophate (all from Sigma-Aldrich) (Zanotti, Kalajzic, Aguila, & Canalis, 2014;

Zanotti et al., 2011, 2013). Cell extracts were obtained for RNA determinations or cultures were stained with alizarin red to assess mineralization.

Quantitative Reverse Transcription-PCR (qRT-PCR)

Total RNA was extracted from cells with the RNeasy kit (Qiagen, Valencia, CA) in accordance with manufacturer's instructions (Canalis et al., 2016; Canalis et al., 2018; Nazarenko, Lowe, et al., 2002; Nazarenko, Pires, Lowe, Obaidy, & Rashtchian, 2002). Equal amounts of RNA were reverse-transcribed using the iScript RT-PCR kit (BioRad, Carlsbad, CA) and amplified in the presence of specific primers (all primers from Integrated DNA Technologies, Coralville, IA; Table 1) with the iQSYBR Green Supermix or SsoAdvanced™ Universal SYBR Green Supermix (BioRad) at 60°C for 40 cycles. Copy number was determined by comparison with a serial dilution of cDNA for *Nfatc1* (Addgene plasmid 11793), *Nfatc2* (Addgene plasmid 11791) (both from A. Rao, La Jolla, CA), *Bglap* (J. Lian, Burlington, VT), *Alpl* and *Rpl38* (American Type Culture Collection, ATCC, Manassas, VA). Amplification reactions were conducted in CFX96 qRT-PCR detection systems (BioRad), and fluorescence was monitored during every PCR cycle at the annealing step. Data are expressed as copy number corrected for *Rpl38* expression (Kouadjo, Nishida, Cadrin-Girard, Yoshioka, & St-Amand, 2007).

Statistics

Data are reported as means ± S.D. Statistical differences were determined by unpaired Student's *t*-test or 2-way analysis of variance with Holm-Šidák post-hoc analysis for pairwise or multiple comparisons.

RESULTS

General Characteristics of Nfatc1 and Nfatc2 Single and Dual Inactivation in Mature Osteoblasts

To study the consequences of the inactivation of *Nfatc1* and *Nfatc2* in the osteoblast lineage, the $Nfatc1^{loxP}$, $Nfatc2^{loxP}$ or both alleles were introduced into *BGLAP-Cre* heterozygous mice. Subsequently, *BGLAP-Cre;*$Nfatc1^{loxP/loxP}$, *BGLAP-Cre;*$Nfatc2^{loxP/loxP}$ or *BGLAP-Cre;*$Nfatc1^{loxP/loxP}$;$Nfatc2^{loxP/loxP}$ mice were crossed with $Nfatc1^{loxP/loxP}$, $Nfatc2^{loxP/loxP}$ or $Nfatc1^{loxP/loxP}$;$Nfatc2^{loxP/loxP}$ mice, respectively, to obtain *BGLAP-Cre;*$Nfatc1^{\Delta/\Delta}$, *BGLAP-Cre;*$Nfatc2^{\Delta/\Delta}$ and *BGLAP-Cre;*$Nfatc1^{\Delta/\Delta}$;$Nfatc2^{\Delta/\Delta}$ test mice and respective $Nfatc^{loxP/loxP}$ control littermates. *BGLAP-Cre;*$Nfatc1^{\Delta/\Delta}$, $Nfatc2^{\Delta/\Delta}$ and $Nfatc1^{\Delta/\Delta}$;$Nfatc2^{\Delta/\Delta}$ mice had a healthy appearance and their weight was comparable to the weight of control mice (Figure 1). *BGLAP-Cre*-dependent recombination was demonstrated in genomic DNA extracted from tibiae of *BGLAP-Cre;*$Nfatc1^{\Delta/\Delta}$, or calvariae of $Nfatc2^{\Delta/\Delta}$ and $Nfatc1^{\Delta/\Delta}$;$Nfatc2^{\Delta/\Delta}$ mice.

Vertebral Microarchitecture and Histomorphometry of Nfatc1 and Nfatc2 Inactivated Mice

Vertebral microarchitecture of 3 month old *BGLAP-Cre;*$Nfatc1^{\Delta/\Delta}$ and 4 month old *BGLAP-Cre;*$Nfatc2^{\Delta/\Delta}$ male and female mice revealed a mild decrease in trabecular bone volume when compared to $Nfatc1^{loxP/loxP}$ or $Nfatc2^{loxP/loxP}$ sex-matched littermate controls (Table 2). To rule out the possibility of genetic compensation between *Nfatc1* and *Nfatc2*,

vertebral microarchitecture was examined in mice harboring the dual deletion of *Nfatc1* and *Nfatc2* in *Bglap*-expressing cells. Vertebral microarchitecture of 4 month old male (Figure 2) and female (Figure 3) *BGLAP-Cre;Nfatc1$^{\Delta/\Delta}$;Nfatc2$^{\Delta/\Delta}$* mice demonstrated a 21% and a 27% decrease in bone volume/total volume when compared to sex-matched littermate controls. This decrease was associated with a significant decrease in trabecular number and connectivity density whereas trabecular thickness was not affected. SMI was increased demonstrating a tendency toward rod-like weaker trabeculae. Female mice harboring *BGLAP-Cre;Nfatc1$^{\Delta/\Delta}$;Nfatc2$^{\Delta/\Delta}$* alleles also were osteopenic at 1 month of age (Figure 3) whereas mature male mice were osteopenic but at 1 month of age had L3 microarchitecture comparable to controls (Figure 2). Bone histomorphometry confirmed the osteopenic phenotype and demonstrated that *BGLAP-Cre;Nfatc1$^{\Delta/\Delta}$;Nfatc2$^{\Delta/\Delta}$* male mice had a significant decrease in osteoblast number and osteoblast and osteoid surface but neither osteoclast number nor eroded surface were affected revealing normal bone resorption (Table 3, Figure 4). Histomorphometric analysis of L3 from *BGLAP-Cre;Nfatc1$^{\Delta/\Delta}$;Nfatc2$^{\Delta/\Delta}$* 4 month old female mice revealed similar trends as male mice, but histomorphometric parameters were not significantly different from controls ($p > 0.05$; not shown).

Femoral Microarchitecture of Nfatc1 and Nfatc2 Inactivated Mice

In contrast to the osteopenic vertebral phenotype of *Nfatc1* and *Nfatc2* null mice, femoral architecture of 1, 3 and 6 month old male and female *BGLAP-Cre;Nfatc1$^{\Delta/\Delta}$* mice revealed no phenotypic differences compared to *Nfatc1$^{loxP/loxP}$* sex-matched littermate controls (Table 4). Similarly, femoral microarchitecture of 1 and 4 month old male and female *BGLAP-Cre;Nfatc2$^{\Delta/\Delta}$* revealed no differences in either cancellous or cortical bone when compared to *Nfatc2$^{loxP/loxP}$* sex-matched littermate controls (Table 5). In addition, the femoral microarchitecture of the dual *Nfatc1;Nfatc2* deletion in *Bglap*-expressing cells demonstrated no appreciably differences in either trabecular or cortical bone between male and female 1 and 4 month old *BGLAP-Cre;Nfatc1$^{\Delta/\Delta}$;Nfatc2$^{\Delta/\Delta}$* and sex-matched *Nfatc1$^{loxP/loxP}$;Nfatc2$^{loxP/loxP}$* littermate controls (Table 6).

Bone Marrow Stromal Cell Cultures from Nfatc1 and Nfatc2 Inactivated Mice

To determine whether *Nfatc1* or *Nfatc2* had a direct effect in cells of the osteoblast lineage, osteoblastogenesis was studied in bone marrow stromal cells following the deletion of *Nfatc1* and *Nfatc2*. Bone marrow stromal cells from *Nfatc1$^{loxP/loxP}$;Nfatc2$^{loxP/loxP}$* mice were transduced with Ad-CMV-Cre to delete *Nfatc1* and *Nfatc2* and compared to control cultures transduced with Ad-CMV-GFP. The downregulation of *Nfatc1* and *Nfatc2* resulted in a transient increase in *Alpl* and *Bglap* mice at confluence and a more sustained decrease in *Alpl* and *Bglap* mRNA expression as well as a modest decrease in mineralization, as the culture progressed (Figure 5). This confirms that NFATc1 and NFATc2 are required for optimal osteoblast differentiation *in vitro*.

DISCUSSION

In the present work, we explored the direct effects of NFATc1 and NFATc2 on osteoblast function following the inactivation of *Nfatc1* and *Nfatc2*, singly and in combination, in cells of the osteoblast lineage. The inactivation of either *Nfatc1*, *Nfatc2* or *Nfatc1* and *Nfatc2* in

Bglap expressing mature osteoblasts resulted in vertebral osteopenia in mature mice. The osteopenia was observed in mature male and female mice, and was modestly more pronounced in the context of the dual *Nfatc1* and *Nfatc2* deletion. This is to be expected and indicative of possible genetic compensation between the 2 transcription factors. These results would indicate that NFATc1 and NFATc2 are necessary for optimal skeletal homeostasis in cancellous vertebral bone. In contrast to the vertebral osteopenia, femoral bone was not affected by the inactivation of *Nfatc1* and *Nfatc2* singly or in combination. There is not an obvious explanation for the predilection of vertebral sites as a consequence of the *Nfatc1*, *Nfatc2* inactivation. This could possibly be due to the fact that vertebral bodies are mostly constituted by cancellous bone, or is possibly related to different levels of expression of *Nfatc1* and *Nfatc2* in vertebral and femoral bone or in the expression of Cre leading to greater recombination and downregulation of target genes in vertebral bones.

Our findings are in contrast to previous work demonstrating that the downregulation of calcineurin in *Bglap*-expressing cells results in an increase in bone volume and bone formation (Yeo et al., 2007). Although calcineurin is required for NFATc activation, it is possible that the phenotype observed following the osteoblast-specific deletion of *Cnb1*, encoding for calcineurin, is due to actions unrelated to NFATc1 and NFATc2 activation. It is worthy to note that the global inactivation of calcineurin Aα results in osteopenia due to suppressed bone formation, a phenotype that is opposite to the one reported for the conditional deletion of *Cnb1* in osteoblasts and more in line with the present work (Sun et al., 2005). The disparity in the results obtained between the two models of calcineurin inactivation may be related to differences in mouse models and in phenotypes achieved following either the global or the cell-specific deletion of the gene in question.

The deletion of *Nfatc1*and *Nfatc2* in cells of the osteoblast lineage resulted in a decrease in osteoblast gene markers *in vitro*, and these results are in accordance with the osteopenic phenotype observed at vertebral sites *in vivo*, and the decreased number of osteoblasts observed in mature male *BGLAP-Cre;Nfatc1*$^{\Delta/\Delta}$*;Nfatc2*$^{\Delta/\Delta}$ mice. The results would suggest that the osteopenia is secondary to decreased osteoblast function/differentiation. Although the number of osteoblasts as well as osteoid surface were decreased in *BGLAP-Cre;Nfatc1*$^{\Delta/\Delta}$*;Nfatc2*$^{\Delta/\Delta}$ mice, mineralizing surface and bone formation were modestly (35%) and not significantly reduced. This is possible due to a modest and somewhat variable affect but may also reflect that NFATc1 and NFATc2 play a limited role in the regulation of bone formation. Our findings are different than those obtained following the downregulation of calcineurin in cells of the osteoblast lineage (Yeo et al., 2007). The deletion of *Cnb1* in osteoblasts resulted in an increase in *Bglap*, *Col1a1* and *Alpl* mRNA levels suggesting that *Cnb1* suppresses osteoblast function (Yeo et al., 2007). Contrary to these results, we find that NFATc1 in combination with NFATc2 are necessary for optimal osteoblast function, since their inactivation results in a decrease in *Alpl* and *Bglap* expression. An explanation for the discrepant results is that the phenotype obtained by the downregulation of *Cnb1* may be due to an alteration in the expression or function of calcineurin-dependent genes other than *Nfatc1*or *Nfatc2*.

Our results are more in line with work in *Nfatc1* and *Cnb1* null mice demonstrating a stimulatory role of NFATc1 in bone formation. However, these studies analyzed the

phenotype of global *Nfatc1* null mice, and the effects in osteoblasts could have been modified by changes in function and behavior of a variety of skeletal and non-skeletal cells affected by the NFATc1 deficiency leading to osteopenia in *Nfatc1* and *Cnb1* null mice (Sun et al., 2005; Winslow et al., 2006). The decrease in osteoblast gene expression observed in *Nfatc1;Nfatc2* deficient osteoblasts is in line with previous work showing that NFATs cooperate with osterix to regulate bone formation in osteoblasts (Koga et al., 2005).

The inactivation of *Nfatc1* and *Nfatc2* in osteoblasts results in a vertebral skeletal phenotype characterized by osteopenia demonstrating that NFATc1 and NFATc2 are necessary for optimal skeletal homeostasis. However, delivery of caNFATc2 to *Col1a1*-expressing osteoblastic cells causes femoral bone osteopenia secondary to decreased bone formation (Zanotti & Canalis, 2015). This inhibitory role of NFATc2 might be attributed to the forced overexpression of the constitutively active form of the transcriptional regulator. It is possible that under basal conditions, NFATc2 has a role in the maintenance of osteoblast function but its overexpression at supraphysiological levels results in an inhibitory effect.

NFATc1 and NFATc2 are physiologically relevant to chondrogenesis. NFATc1 and NFATc2 are repressors of chondrogenesis and cartilage growth. Deletion of *Nfatc2* leads to the ectopic formation of cartilage surrounding synovial tissue and to the development of osteoarthritis particularly when associated with the deletion of *Nfatc1* (Greenblatt et al., 2013; Ranger et al., 1998; Rodova et al., 2011). Most of the manifestations of the disruption of *Nfatc2* appear in postnatal and adult life since *Nfatc2* is not expressed during the early developmental stages of cartilage formation (Ranger et al., 1998). NFATc1 and NFATc2 play a restrictive role in osteochondral growth, and as a consequence their inactivation leads to entheseal osteochondromas (Ge et al., 2016).

The observations may suggest a more important function of NFATc1 and NFATc2 in chondrocytes than in mature osteoblasts (Zanotti et al., 2011, 2013). However, our results do not exclude a more pronounced effect of NFATc1 and NFATc2 early in the osteoblastogenesis program since the *BGLAP* promoter used to direct Cre-dependent deletion of *Nfatc1* and *Nfatc2* is expressed in mature osteoblasts (Matthews et al., 2016).

Recently, we reported that a mouse model of Hajdu Cheney Syndrome associated with a NOTCH2 gain-of-function is sensitized to the development of osteoarthritis (Zanotti, Yu, Bridgewater, Wolf, & Canalis, 2018). Notch signaling represses *Nfatc1*, but induces *Nfatc2* by post-transcriptional mechanisms and it is possible that the NFATc2 induction acts as a mechanism to protect joint integrity (Greenblatt et al., 2013; Zanotti & Canalis, 2013; Zanotti et al., 2011, 2013). NFATc1 and NFATc2 interact with Notch signaling in osteoblasts and compete with the Notch transcriptional complex for binding to DNA with a consequent downregulation of Notch signaling (Zanotti et al., 2013). The inactivation of *Nfatc1* and *Nfatc2* in bone marrow stromal cells resulted in a downregulation of *Hey1* expression without a decrease in *Hey2*, *HeyL* and *Hes1* expression (data not shown). This would suggest that the decrease in *Hey1* mRNA is independent of a generalized downregulation of Notch signaling, and that Notch signaling is not significantly affected under conditions of *Nfatc* inactivation as it is under conditions of NFATc overexpression.

CONCLUSIONS

In conclusion, the present work demonstrates that NFATc1 and NFATc2 are necessary for optimal osteoblast differentiation and function and the maintenance of skeletal homeostasis at vertebral but not femoral sites.

ACKNOWLEDGMENTS

The authors thank J. Lian for *Bglap* cDNA, A. Rao for *Nfatc1* and *Nfatc2* cDNA, and Sarah Bosco and Mary Yurczak for assistance.

This work was supported by grant AR068160 (EC) from the National Institute of Arthritis and Musculoskeletal and Skin Diseases. The content is solely the responsibility of the authors and does not necessarily represent the official views of the National Institutes of Health.

REFERENCES

Aliprantis AO, Ueki Y, Sulyanto R, Park A, Sigrist KS, Sharma SM, … Glimcher LH (2008). NFATc1 in mice represses osteoprotegerin during osteoclastogenesis and dissociates systemic osteopenia from inflammation in cherubism. The Journal of clinical investigation, 118(11), 3775–3789. [PubMed: 18846253]

Asagiri M, Sato K, Usami T, Ochi S, Nishina H, Yoshida H, … Takayanagi H (2005). Autoamplification of NFATc1 expression determines its essential role in bone homeostasis. Journal of Experimental Medicine, 202(9), 1261–1269. [PubMed: 16275763]

Bauer W, Rauner M, Haase M, Kujawski S, Arabanian LS, Habermann I, … Kiani A (2011). Osteomyelosclerosis, anemia and extramedullary hematopoiesis in mice lacking the transcription factor NFATc2. Haematologica, 96(11), 1580–1588. doi:10.3324/haematol.2011.042515 [PubMed: 21750088]

Bianco P, & Gehron RP (2000). Marrow stromal stem cells. The Journal of clinical investigation, 105(12), 1663–1668. [PubMed: 10862779]

Bouxsein ML, Boyd SK, Christiansen BA, Guldberg RE, Jepsen KJ, & Muller R (2010). Guidelines for assessment of bone microstructure in rodents using micro-computed tomography. Journal of Bone and Mineral Research, 25(7), 1468–1486. [PubMed: 20533309]

Canalis E, Schilling L, Yee SP, Lee SK, & Zanotti S (2016). Hajdu Cheney Mouse Mutants Exhibit Osteopenia, Increased Osteoclastogenesis and Bone Resorption. Journal of Biological Chemistry, 291, 1538–1551. doi:10.1074/jbc.M115.685453 [PubMed: 26627824]

Canalis E, Yu J, Schilling L, Yee SP, & Zanotti S (2018). The lateral meningocele syndrome mutation causes marked osteopenia in mice. Journal of Biological Chemistry, 293(36), 14165–14177. doi:10.1074/jbc.RA118.004242 [PubMed: 30042232]

Chow W, Hou G, & Bendeck MP (2008). Glycogen synthase kinase 3beta regulation of nuclear factor of activated T-cells isoform c1 in the vascular smooth muscle cell response to injury. Experimental Cell Research, 314(16), 2919–2929. [PubMed: 18675800]

Crabtree GR, & Olson EN (2002). NFAT signaling: choreographing the social lives of cells. Cell, 109 Suppl, S67–S79. [PubMed: 11983154]

Dempster DW, Compston JE, Drezner MK, Glorieux FH, Kanis JA, Malluche H, … Parfitt AM (2013). Standardized nomenclature, symbols, and units for bone histomorphometry: a 2012 update of the report of the ASBMR Histomorphometry Nomenclature Committee. Journal of Bone and Mineral Research, 28(1), 2–17. doi:10.1002/jbmr.1805 [doi] [PubMed: 23197339]

Ge X, Tsang K, He L, Garcia RA, Ermann J, Mizoguchi F, … Aliprantis AO (2016). NFAT restricts osteochondroma formation from entheseal progenitors. JCI Insight, 1(4), e86254. doi:10.1172/jci.insight.86254 [PubMed: 27158674]

Glatt V, Canalis E, Stadmeyer L, & Bouxsein ML (2007). Age-Related Changes in Trabecular Architecture Differ in Female and Male C57BL/6J Mice. Journal of Bone and Mineral Research, 22(8), 1197–1207. [PubMed: 17488199]

Graef IA, Chen F, & Crabtree GR (2001). NFAT signaling in vertebrate development. Curr. Opin. Genet Dev, 11(5), 505–512. [PubMed: 11532391]

Greenblatt MB, Ritter SY, Wright J, Tsang K, Hu D, Glimcher LH, & Aliprantis AO (2013). NFATc1 and NFATc2 repress spontaneous osteoarthritis1. Proceedings of the National Academy of Sciences of the United States of America, 110(49), 19914–19919. doi:1320036110 [pii];10.1073/pnas.1320036110 [doi] [PubMed: 24248346]

Hogan PG, Chen L, Nardone J, & Rao A (2003). Transcriptional regulation by calcium, calcineurin, and NFAT. Genes & Development, 17(18), 2205–2232. [PubMed: 12975316]

Ikeda F, Nishimura R, Matsubara T, Hata K, Reddy SV, & Yoneda T (2006). Activation of NFAT signal in vivo leads to osteopenia associated with increased osteoclastogenesis and bone-resorbing activity. Journal of Immunology, 177(4), 2384–2390.

Ikeda F, Nishimura R, Matsubara T, Tanaka S, Inoue J, Reddy SV, … Yoneda T (2004). Critical roles of c-Jun signaling in regulation of NFAT family and RANKL-regulated osteoclast differentiation. Journal of Clinical Investigation, 114(4), 475–484. doi:10.1172/JCI19657 [PubMed: 15314684]

Ishida N, Hayashi K, Hoshijima M, Ogawa T, Koga S, Miyatake Y, … Takeya T (2002). Large scale gene expression analysis of osteoclastogenesis in vitro and elucidation of NFAT2 as a key regulator. Journal of Biological Chemistry, 277(43), 41147–41156. doi:10.1074/jbc.M205063200 [PubMed: 12171919]

Koga T, Matsui Y, Asagiri M, Kodama T, d. C. B, Nakashima K, & Takayanagi H (2005). NFAT and Osterix cooperatively regulate bone formation. Nature Medicine, 11(8), 880–885.

Kouadjo KE, Nishida Y, Cadrin-Girard JF, Yoshioka M, & St-Amand J (2007). Housekeeping and tissue-specific genes in mouse tissues. BMC Genomics, 8, 127. doi:10.1186/1471-2164-8-127 [PubMed: 17519037]

Matsuo K, Galson DL, Zhao C, Peng L, Laplace C, Wang KZ, … Wagner EF (2004). Nuclear factor of activated T-cells (NFAT) rescues osteoclastogenesis in precursors lacking c-Fos. Journal of Biological Chemistry, 279(25), 26475–26480. doi:10.1074/jbc.M313973200 [PubMed: 15073183]

Matthews BG, Roguljic H, Franceschetti T, Roeder E, Matic I, Vidovic I, … Kalajzic I (2016). Gene-expression analysis of cementoblasts and osteoblasts. J Periodontal Res, 51(3), 304–312. doi:10.1111/jre.12309 [PubMed: 26215316]

Nazarenko I, Lowe B, Darfler M, Ikonomi P, Schuster D, & Rashtchian A (2002). Multiplex quantitative PCR using self-quenched primers labeled with a single fluorophore. Nucleic Acids Research, 30(9), e37. [PubMed: 11972352]

Nazarenko I, Pires R, Lowe B, Obaidy M, & Rashtchian A (2002). Effect of primary and secondary structure of oligodeoxyribonucleotides on the fluorescent properties of conjugated dyes. Nucleic Acids Research, 30(9), 2089–2195. [PubMed: 11972350]

Okamura H, Aramburu J, Garcia-Rodriguez C, Viola JP, Raghavan A, Tahiliani M, … Rao A (2000). Concerted dephosphorylation of the transcription factor NFAT1 induces a conformational switch that regulates transcriptional activity. Molecular Cell, 6(3), 539–550. [PubMed: 11030334]

Parfitt AM, Drezner MK, Glorieux FH, Kanis JA, Malluche H, Meunier PJ, … Recker RR (1987). Bone histomorphometry: standardization of nomenclature, symbols, and units. Report of the ASBMR Histomorphometry Nomenclature Committee. Journal of Bone and Mineral Research, 2(6), 595–610. [PubMed: 3455637]

Ranger AM, Gerstenfeld LC, Wang J, Kon T, Bae H, Gravallese EM, … Glimcher LH (2000). The nuclear factor of activated T cells (NFAT) transcription factor NFATp (NFATc2) is a repressor of chondrogenesis. Journal of Experimental Medicine, 191(1), 9–22. [PubMed: 10620601]

Ranger AM, Grusby MJ, Hodge MR, Gravallese EM, de la Brousse FC, Hoey T, … Glimcher LH (1998). The transcription factor NF-ATc is essential for cardiac valve formation. Nature, 392(6672), 186–190. [PubMed: 9515964]

Rodova M, Lu Q, Li Y, Woodbury BG, Crist JD, Gardner BM, … Wang J (2011). Nfat1 regulates adult articular chondrocyte function through its age-dependent expression mediated by epigenetic histone methylation. Journal of Bone and Mineral Research, 26(8), 1974–1986. doi:10.1002/jbmr.397 [PubMed: 21452283]

Sitara D, & Aliprantis AO (2010). Transcriptional regulation of bone and joint remodeling by NFAT. Immunological Reviews, 233(1), 286–300. [PubMed: 20193006]

Sun L, Blair HC, Peng Y, Zaidi N, Adebanjo OA, Wu XB, … Zaidi M (2005). Calcineurin regulates bone formation by the osteoblast. Proceedings of the National Academy of Sciences of the United States of America, 102(47), 17130–17135. [PubMed: 16286645]

Takayanagi H, Kim S, Koga T, Nishina H, Isshiki M, Yoshida H, … Taniguchi T (2002). Induction and activation of the transcription factor NFATc1 (NFAT2) integrate RANKL signaling in terminal differentiation of osteoclasts. Dev Cell, 3(6), 889–901. [PubMed: 12479813]

Winslow MM, Pan M, Starbuck M, Gallo EM, Deng L, Karsenty G, & Crabtree GR (2006). Calcineurin/NFAT signaling in osteoblasts regulates bone mass. Developmental Cell, 10(6), 771–782. [PubMed: 16740479]

Yeo H, Beck LH, Thompson SR, Farach-Carson MC, McDonald JM, Clemens TL, & Zayzafoon M (2007). Conditional disruption of calcineurin B1 in osteoblasts increases bone formation and reduces bone resorption. Journal of Biological Chemistry, 282(48), 35318–35327. [PubMed: 17884821]

Yu J, Zanotti S, Schilling L, & Canalis E (2018). Nuclear factor of activated T cells 2 is required for osteoclast differentiation and function in vitro but not in vivo. Journal of Cellular Biochemistry, 119(11), 9334–9345. doi:10.1002/jcb.27212 [PubMed: 30010214]

Zanotti S, & Canalis E (2013). Notch suppresses nuclear factor of activated T cells (Nfat) transactivation and Nfatc1 expression in chondrocytes. Endocrinology, 154(2), 762–772. doi:en.2012–1925 [pii];10.1210/en.2012-1925 [doi] [PubMed: 23264614]

Zanotti S, & Canalis E (2015). Activation of Nfatc2 in Osteoblasts Causes Osteopenia. Journal of Cellular Physiology, 230(7), 1689–1695. doi:10.1002/jcp.24928 [PubMed: 25573264]

Zanotti S, Kalajzic I, Aguila HL, & Canalis E (2014). Sex and genetic factors determine osteoblastic differentiation potential of murine bone marrow stromal cells. PLoS One, 9(1), e86757. doi:10.1371/journal.pone.0086757 [doi];PONE-D-13–31354 [pii] [PubMed: 24489784]

Zanotti S, Smerdel-Ramoya A, & Canalis E (2011). Reciprocal regulation of Notch and nuclear factor of activated T-cells (NFAT) c1 transactivation in osteoblasts. Journal of Biological Chemistry, 286(6), 4576–4588. doi:10.1074/jbc.M110.161893 [PubMed: 21131365]

Zanotti S, Smerdel-Ramoya A, & Canalis E (2013). Nuclear Factor of Activated T-cells (Nfat)c2 Inhibits Notch Signaling in Osteoblasts. Journal of Biological Chemistry, 288(1), 624–632. doi:M112.340455 [pii];10.1074/jbc.M112.340455 [doi] [PubMed: 23166323]

Zanotti S, Yu J, Bridgewater D, Wolf JM, & Canalis E (2018). Mice harboring a Hajdu Cheney Syndrome mutation are sensitized to osteoarthritis. Bone, 114, 198–205. doi:10.1016/j.bone.2018.06.020 [PubMed: 29940267]

Zhang M, Xuan S, Bouxsein ML, von Stechow D, Akeno N, Faugere MC, … Clemens TL (2002). Osteoblast-specific knockout of the insulin-like growth factor (IGF) receptor gene reveals an essential role of IGF signaling in bone matrix mineralization. Journal of Biological Chemistry, 277(46), 44005–44012. [PubMed: 12215457]

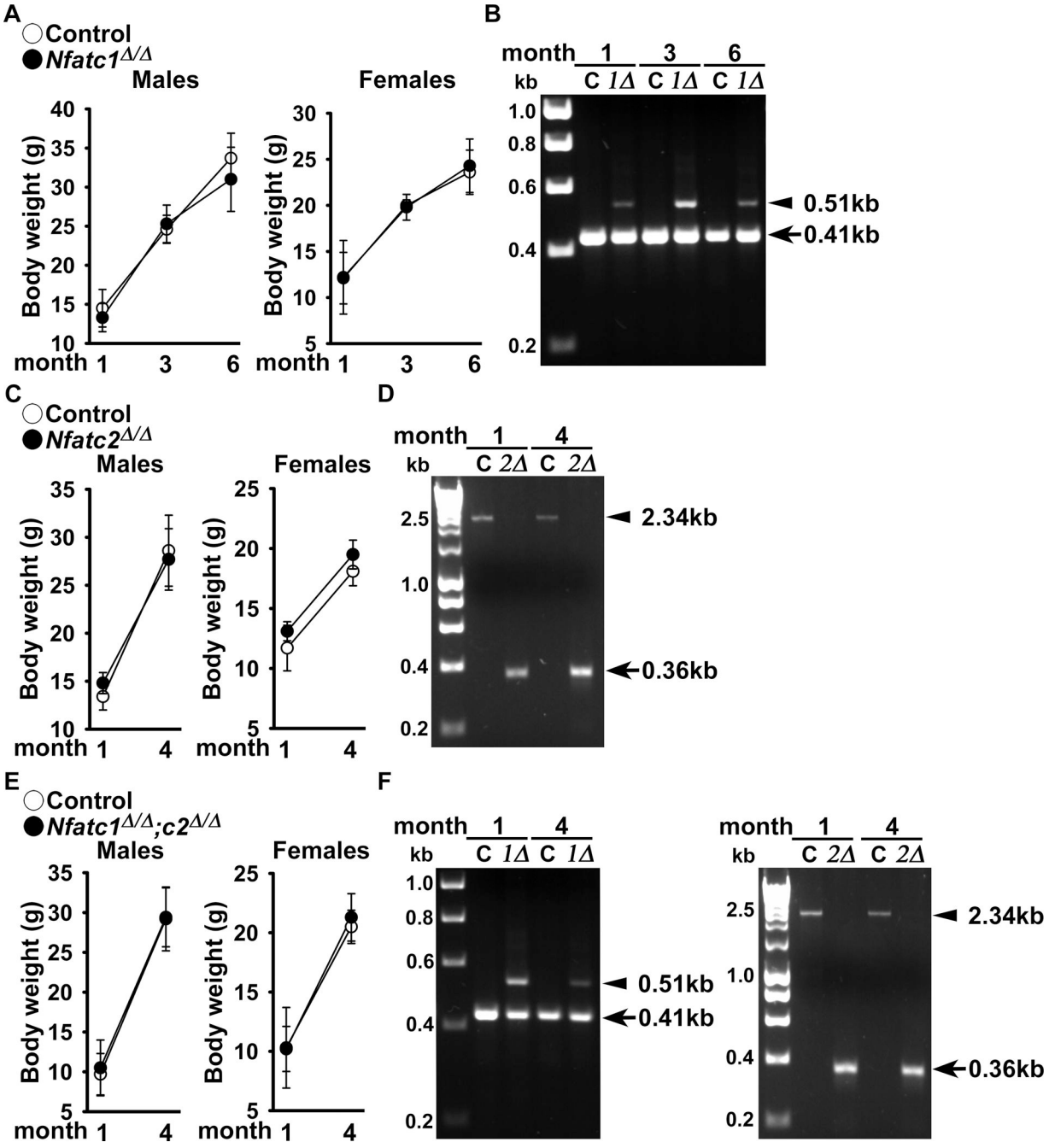

Figure 1.

Weight and documentation of DNA recombination of *Nfatc1* and *Nfatc2* alleles by *BGLAP*-driven Cre. (A) Body weight of *BGLAP-Cre;Nfatc1*$^{\Delta/\Delta}$, *BGLAP-Cre;Nfatc2*$^{\Delta/\Delta}$ and *BGLAP-Cre;Nfatc1*$^{\Delta/\Delta}$;*Nfatc2*$^{\Delta/\Delta}$ and sex-matched control *Nfatc1*$^{loxP/loxP}$, *Nfatc2*$^{loxP/loxP}$ and *Nfatc1*$^{loxP/loxP}$;*Nfatc2*$^{loxP/loxP}$ littermates. Values are means ± SD; n = 3 control and n = 6 *Nfatc1*$^{\Delta/\Delta}$; n = 5 control and n = 7 *Nfatc2*$^{\Delta/\Delta}$ and n = 3 control and n= 9 *Nfatc1*$^{\Delta/\Delta}$;*Nfatc2*$^{\Delta/\Delta}$. (B) DNA from tibiae were obtained from *BGLAP-Cre;Nfatc1*$^{\Delta/\Delta}$ and DNA from calvariae were obtained from *BGLAP-Cre;Nfatc2*$^{\Delta/\Delta}$ and from *BGLAP-Cre;Nfatc1*$^{\Delta/\Delta}$;*Nfatc2*$^{\Delta/\Delta}$ neonates and from their respective (non-Cre) *Nfatc1*$^{loxP/loxP}$,

Nfatc2$^{loxP/loxP}$ and *Nfatc1*$^{loxP/loxP}$;*Nfatc2*$^{loxP/loxP}$ controls. Cre-dependent DNA recombination was demonstrated by gel electrophoresis of PCR amplification products obtained with primers for the unrecombined *Nfatc1*^{loxP} and *Nfatc2*^{loxP} and for the Cre-mediated recombined *Nfatc1*$^{\Delta}$ and *Nfatc2*$^{\Delta}$ alleles. In Figure 1B and 1F left, the arrow heads indicate the position of the 410 base pair (bp) amplicon verifying the unrecombined *Nfatc1*^{loxP} allele and 510 bp amplicon verifying the Cre-mediated recombined *Nfatc1*$^{\Delta}$ allele. In Figure 1D and right, the arrow heads indicate the 2.3 kilobase (kb) amplicon verifying the unrecombined *Nfatc2*^{loxP} allele, and the 0.36 kb amplicon verifying the Cre-mediated recombined *Nfatc2*$^{\Delta}$ allele.

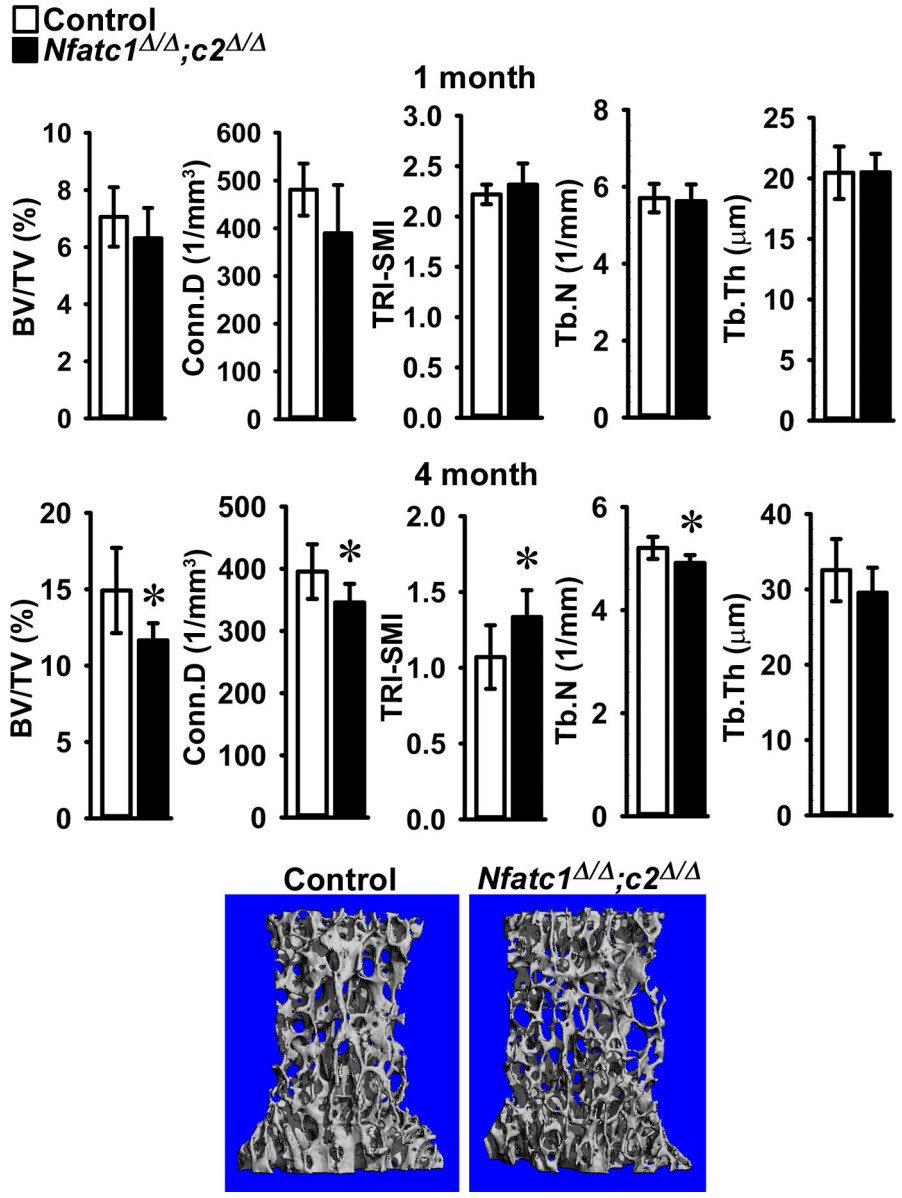

Figure 2.

Cancellous bone microarchitecture assessed by μCT of vertebral body of Lumbar 3 (L3) from 1 (upper panels) and 4 (lower panels) month old *BGLAP-Cre;Nfatc1*$^{\Delta/\Delta}$*;Nfatc2*$^{\Delta/\Delta}$ male mice (black bars) and sex-matched littermate *Nfatc1*$^{loxP/loxP}$*;Nfatc2*$^{loxP/loxP}$ controls (white bars). Parameters shown are: bone volume/tissue volume (BV/TV); connectivity density (Conn.D); structure model index (SMI); trabecular number (Tb.N) and trabecular thickness (Tb,Th). Values are means ± SD; n = 5 to 6 for control and n = 6 to 9 for *Nfatc1*$^{\Delta/\Delta}$*;Nfatc2*$^{\Delta/\Delta}$ mice. A representative image shows cancellous bone osteopenia in 4 month old *BGLAP-Cre;Nfatc1*$^{\Delta/\Delta}$*;Nfatc2*$^{\Delta/\Delta}$ male mice.

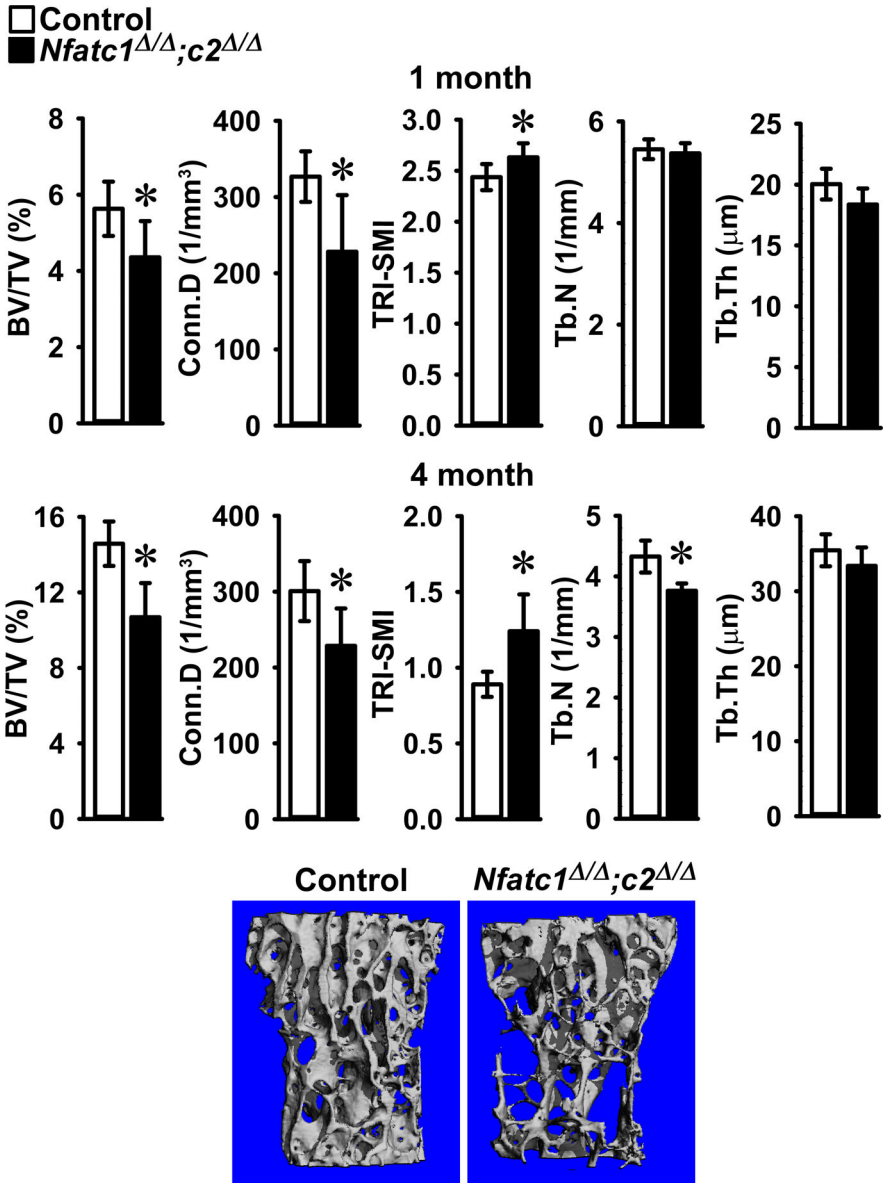

Figure 3.

Cancellous bone microarchitecture assessed by μCT of vertebral body of Lumbar 3 (L3) from 1 (upper panels) and 4 (lower panels) month old *BGLAP-Cre;Nfatc1*$^{\Delta/\Delta}$*;Nfatc2*$^{\Delta/\Delta}$ female mice (black bars) and sex-matched littermate *Nfatc1*$^{loxP/loxP}$*;Nfatc2*$^{loxP/loxP}$ controls (white bars). Parameters shown are: bone volume/tissue volume (BV/TV); connectivity density (Conn.D); structure model index (SMI); trabecular number (Tb.N) and trabecular thickness (Tb.Th). Values are means ± SD; n = 5 for control and n = 8 for *Nfatc1*$^{\Delta/\Delta}$*;Nfatc2*$^{\Delta/\Delta}$ mice. A representative image shows cancellous bone osteopenia in 4 month old *BGLAP-Cre;Nfatc1*$^{\Delta/\Delta}$*;Nfatc2*$^{\Delta/\Delta}$ female mice.

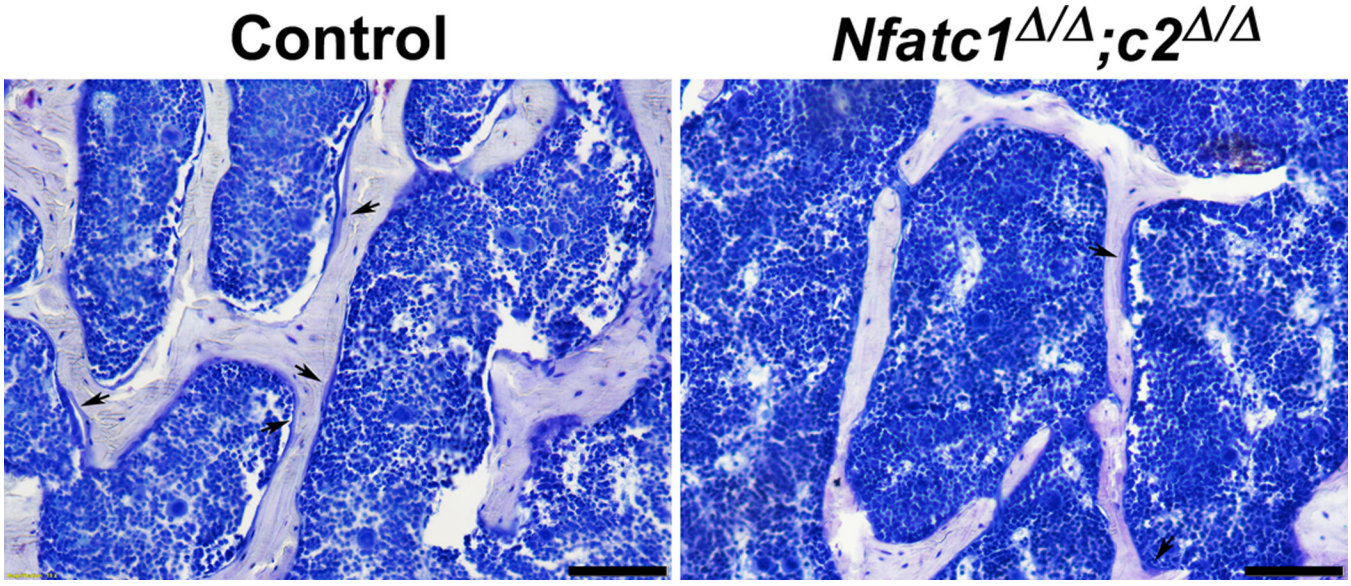

Figure 4.

Representative image of bone histomorphometry from 4 month old *BGLAP-Cre;Nfatc1*$^{\Delta/\Delta}$*;Nfatc2*$^{\Delta/\Delta}$ male mice and control littermates. Sections were stained with toluidine blue. Arrows point to osteoblasts on osteoid surfaces and bar in right corner represents 100 μm.

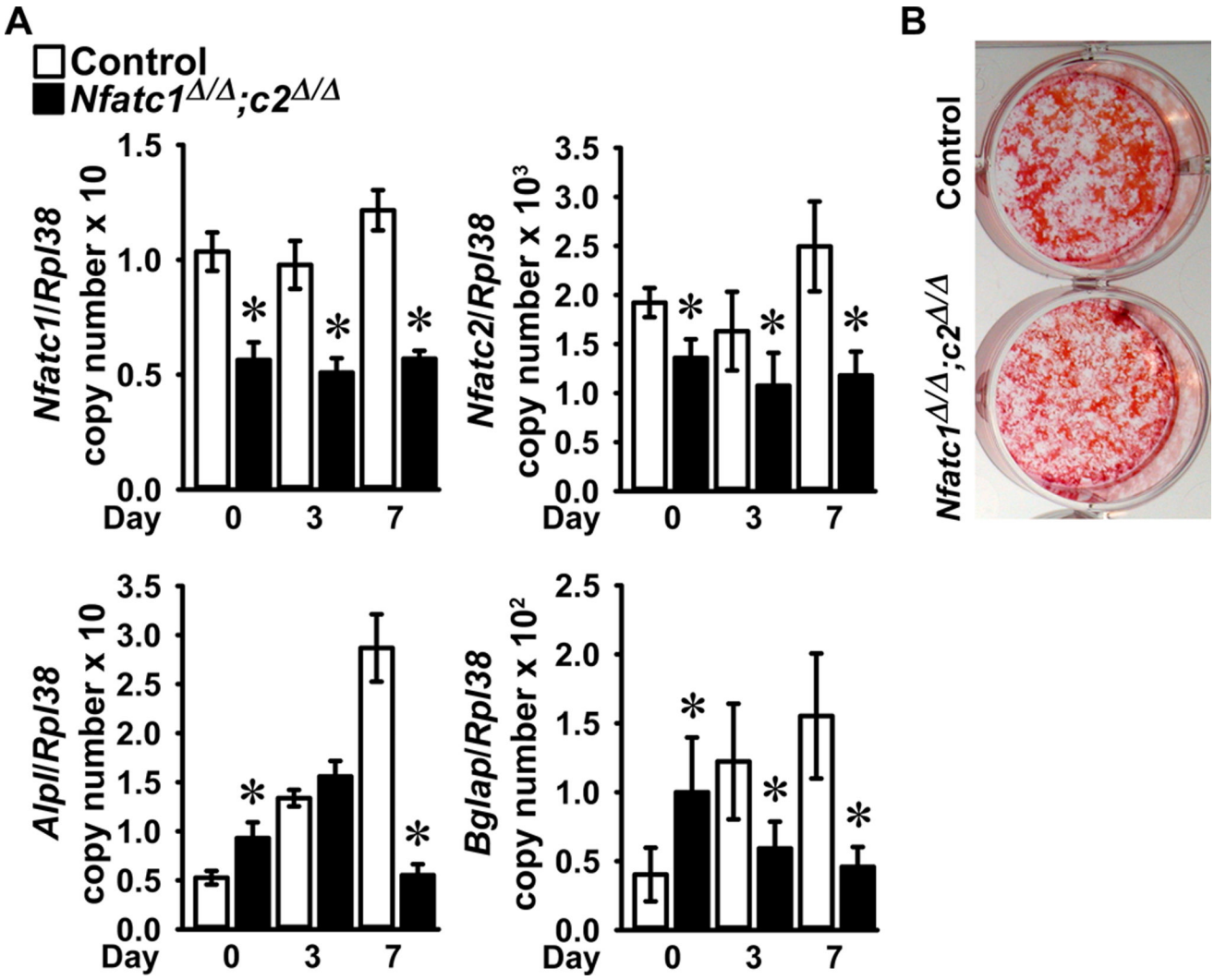

Figure 5.

Bone marrow stromal cells harvested from femurs of 6 to 8 week old male *Nfatc1*$^{loxP/loxP}$;*Nfatc2*$^{loxP/loxP}$ mice were cultured to subconfluence, transduced with Ad-CMV-Cre (*Nfatc1*$^{\Delta/\Delta}$;*Nfatc2*$^{\Delta/\Delta}$, black bars) or Ad-CMV-GFP (control, white bars) and cultured under conditions favoring osteoblastogenesis following confluence (Day 0). In Panel A, total RNA was extracted and gene expression determined by qRT-PCR. Data are expressed as *Nfatc1*, *Nfatc2*, *Alpl* and *Bglap* copy number corrected for *Rpl38* copy number. Values are means ± SD; n = 4. *Significantly different between *Nfatc1*$^{\Delta/\Delta}$;*Nfatc2*$^{\Delta/\Delta}$ and control, $p < 0.05$. In Panel B, a representative image shows control and *Nfatc1*$^{\Delta/\Delta}$;*Nfatc2*$^{\Delta/\Delta}$ 14 day cultures stained with alizarin red.

Table 1.

Primers used for allele identification and for qRT-PCR.

A. rimers for allele identification and DNA recombination			
Allele	**Strand**	**Sequence**	**Amplicon Size (bp)**
BGLAP-Cre transgene	Forward Reverse	5’-CAAATAGCCCTGCAGAT-3’ 5’-TGATACAAGGGACATCTTCC-3’	300
Nfatc1^{loxP}	Forward Reverse	5’-GGACAGTCTAAGGCCTGCTG-3’ 5’-ACCCCACATCCCAGAGTGA-3’	*Nfatc1*^{WT} = 215 *Nfatc1*^{loxP} = 300
Nfatc2^{loxP}	Forward Reverse	5’-GGTGTCTCCCTCAAATGTTCA-3’ 5’-GCGAATATGAGGACCCAAGT-3’	*Nfatc2*^{WT} = 160 *Nfatc2*^{loxP}= 250
LoxP recombination of *Nfatc1*^{loxP}	Forward Forward Reverse	5’-AAGGAATTACTGGGAAGCCTGGCA-3’ 5’-AGGGACTATCATTTGGCAGGGACA-3’ 5’-ACAGGAAACAGCTCTGTTCCACAC-3’	Recombined = 510 (*Nfatc1*$^{\Delta}$) Not recombined = 410 (*Nfatc1*^{loxP})
LoxP recombination of *Nfatc2*^{loxP}	Forward Reverse	5’-AGCACAATGCCCATGTTCAC-3’ 5’-GGTGTCTCCCTCAAATGTTCA-3’	Recombined = 358 (*Nfatc2*$^{\Delta}$) Not recombined = 2342 (*Nfatc2*^{loxP})

B. Primers for qRT-PCR and GenBank accession numbers for the transcript variants recognized by primer pairs			
Gene	**Strand**	**Primer Sequence**	**GenBank Accession Number**
Alp1	Forward Reverse	5’-CGGTTAGGGCGTCTCCACAGTAAC[FAM]G-3’ 5’-CTTGGAGAGGGCCACAAAGG-3’	NM_007431
Bglap	Forward Reverse	5’-GACTCCGGCGCTACCTTGGGTAAG-3’ 5’-CCCAGCACAACTCCTCCCTA-3’	NM_001037939
Nfatc1	Forward Reverse	5’-GCGCAAGTACAGTCTCAATGGCC-3’ 5’-GGATGGTGTGGGTGAGTGGT-3’	NM_198429; NM_001164110; NM_001164111; NM_001164112; NM_00116641091; NM_016791
Nfatc2	Forward Reverse	5’-AGAACAACATGAGAGCCACCATC-3’ 5’-AGCTCGATGTCAGCGTTTCG-3’	NM_010899
Rpl38	Forward Reverse	5’-AGAACAAGGATAATGTGAAGTTCAAGGTTC-3’ 5’-CTGCTTCAGCTTCTCTGCCTTT-3’	NM_001048057; NM_001048058; NM_023372

Table 2.

Lumbar 3 (L3) assessed by μCT of *BGLAP-Cre;Nfatc1*$^{\Delta/\Delta}$ and *BGLAP-Cre;Nfatc2*$^{\Delta/\Delta}$ male and female mice and sex-matched *Nfatc1*$^{loxP/loxP}$ or *Nfatc2*$^{loxP/loxP}$ littermate controls.

Nfatc1	**Males**		**Females**	
	Control n = 8	***Nfatc1*$^{\Delta/\Delta}$ n = 8**	**Control n = 9**	***Nfatc1*$^{\Delta/\Delta}$ n = 6**
Distal Femur Trabecular Bone				
Bone Volume/Total Volume (%)	12.6 ± 0.9	10.8 ± 1.4 *	13.0 ± 2.0	10.9 ± 1.0 *
Trabecular Separation (μm)	185 ± 9	187 ± 10	220 ± 10	239 ± 14 *
Trabecular Number (1/mm)	5.2 ± 0.3	5.2 ± 0.3	4.5 ± 0.2	4.1 ± 0.2 *
Trabecular Thickness (μm)	28 ± 1	26 ± 1 *	31 ± 3	31 ± 1
Connectivity Density (1/mm^3)	418 ± 48	422 ± 52	380 ± 72	306 ± 63
Structure Model Index	1.2 ± 0.1	1.4 ± 0.1 *	1.2 ± 0.3	1.3 ± 0.1
Density of Material (mg HA/cm^3)	947 ± 11	960 ± 21	928 ± 33	938 ± 10

Nfatc2	**Males**		**Females**	
	Control n = 8	***Nfatc2*$^{\Delta/\Delta}$ n = 9**	**Control n = 8**	***Nfatc2*$^{\Delta/\Delta}$ n = 8**
Distal Femur Trabecular Bone				
Bone Volume/Total Volume (%)	11.3 ± 0.8	10.2 ± 1.3 +	8.3 ± 0.7	6.9 ± 1.2 *
Trabecular Separation (μm)	201 ± 9	199 ± 13	255 ± 16	257 ± 15
Trabecular Number (1/mm)	5.0 ± 0.2	5.0 ± 0.3	4.0 ± 0.3	3.9 ± 0.2
Trabecular Thickness (μm)	29 ± 1	28 ± 2	31 ± 2	28 ± 1 *
Connectivity Density (1/mm^3)	350 ± 44	342 ± 86	237 ± 44	252 ± 70
Structure Model Index	1.3 ± 0.2	1.5 ± 0.2	1.7 ± 0.1	1.9 ± 0.2 *
Density of Material (mg HA/cm^3)	1012 ± 18	1009 ± 22	973 ± 24	977 ± 29

μCT was performed in L3 vertebral bodies from 3 month old male and female *BGLAP-Cre;Nfatc1*$^{\Delta/\Delta}$ mice and 4 month old *BGLAP-Cre;Nfatc2*$^{\Delta/\Delta}$ mice and sex-matched *Nfatc1*$^{loxP/loxP}$ or *Nfatc2*$^{loxP/loxP}$ littermates. Values are means ± SD.

*Significantly different between control and *BGLAP-Cre;Nfatc1*$^{\Delta/\Delta}$ or control and *BGLAP-Cre;Nfatc2*$^{\Delta/\Delta}$, $p < 0.05$ by unpaired *t*-test;

+$p = 0.058$.

Table 3.

Cancellous vertebral histomorphometry of 4 month old *BGLAP-Cre;Nfatc1$^{\Delta/\Delta}$;Nfatc2$^{\Delta/\Delta}$* male mice and littermate controls.

	Control n = 4	***Nfatc1*$^{\Delta/\Delta}$;*2*$^{\Delta/\Delta}$ N = 9**
Bone Volume/Total Volume (%)	22.1 ± 5.4	16.4 ± 4.0 $^{+}$
Trabecular Number (1/mm)	4.5 ± 0.7	3.9 ± 0.8
Trabecular Thickness (μm)	49 ± 6	43 ± 7
Osteoblasts/Bone Perimeter (1/mm)	6.1 ± 0.9	3.4 ± 1.4 *
Osteoblast Surface/Bone Surface (%)	7.7 ± 1.6	4.3 ± 2.0 *
Osteoid Surface/Bone Surface (%)	0.8 ± 0.3	0.1 ± 0.1 *
Osteoclasts/Bone Perimeter (1/mm)	1.6 ± 0.4	2.1 ± 0.8
Eroded Surface/Bone Surface (%)	1.8 ± 0.7	2.1 ± 1.0
Mineral Apposition Rate (μm/day)	0.8 ± 0.2	0.8 ± 0.1
Mineralizing Surface/Bone Surface (%)	2.6 ± 0.7	1.7 ± 1.0
Bone Formation Rate ($\mu m^3/\mu m^2$/day)	0.022 ± 0.01	0.014 ± 0.01

Bone histomorphometry was performed in L3 vertebral bodies from 4 month old male *BGLAP-Cre;Nfatc1$^{\Delta/\Delta}$;Nfatc2$^{\Delta/\Delta}$* mice and sex-matched *Nfatc1$^{loxP/loxP}$;Nfatc2$^{loxP/loxP}$* littermates (control). Values are means ± SD.

*Significantly different between *BGLAP-Cre;Nfatc1$^{\Delta/\Delta}$;Nfatc2$^{\Delta/\Delta}$* and control, $p < 0.05$;

$^{+}$$p$ 0.0547.

Table 4.

Femoral microarchitecture assessed by μCT of 1, 3 and 6 month old male and female *BGLAP;Nfatc1*$^{\Delta/\Delta}$ mice and sex-matched *Nfatc1*$^{loxP/loxP}$ littermate controls.

Males	**1 Month**		**3 Month**		**6 Month**	
	Control n = 4	***Nfatc1*$^{\Delta/\Delta}$ n = 4**	**Control n = 5**	***Nfatc1*$^{\Delta/\Delta}$ n = 5**	**Control n = 6**	***Nfatc1*$^{\Delta/\Delta}$ n = 6**
Distal Femur Trabecular Bone						
Bone Volume/Total Volume (%)	5.9 ± 1.2	5.7 ± 2.1	3.1 ± 1.0	2.9 ± 0.4	2.1 ± 0.2	2.0 ± 0.6
Trabecular Separation (μm)	183 ± 15	180 ± 25	232 ± 10	226 ± 7	270 ± 14	272 ± 23
Trabecular Number (1/mm)	5.5 ± 0.5	5.7 ± 0.9	4.3 ± 0.2	4.4 ± 0.1	3.7 ± 0.2	3.7 ± 0.3
Trabecular Thickness (μm)	21 ± 1	20 ± 1	25 ± 2	23 ± 2	27 ± 2	25 ± 2
Connectivity Density (1/mm^3)	277 ± 130	324 ± 268	46 ± 28	29 ± 22	23 ± 15	26 ± 24
Structure Model Index	3.2 ± 0.1	3.2 ± 0.2	3.2 ± 0.2	3.1 ± 0.1	3.4 ± 0.1	3.4 ± 0.3
Density of Material (mg HA/cm^3)	895 ± 7	895 ± 18	987 ± 10	977 ± 31	1025 ± 18	1040 ± 12
	n = 4	**n = 4**	**n = 4**	**n = 5**	**n = 5**	**n = 6**
Femoral Midshaft Cortical Bone						
Bone Volume/Total Volume (%)	82.9 ± 1.8	81.5 ± 1.3	87.5 ± 0.5	87.1 ± 0.8	89.3 ± 1.1	89.5 ± 0.5
Porosity (%)	17.1 ± 1.8	18.5 ± 1.3	12.5 ± 0.5	12.9 ± 0.8	10.7 ± 1.1	10.5 ± 0.5
Cortical Thickness (μm)	88 ± 10	80 ± 5	152 ± 6	146 ± 9	156 ± 11	153 ± 4
Total Area (mm^2)	1.4 ± 0.1	1.4 ± 0.1	1.7 ± 0.1	1.7 ± 0.1	1.8 ± 0.1	1.7 ± 0.1
Bone Area (mm^2)	0.5 ± 0.1	0.4 ± 0.1	0.8 ± 0.1	0.7 ± 0.1	0.8 ± 0.1	0.8 ± 0.1
Periosteal Perimeter (mm)	4.2 ± 0.1	4.3 ± 0.2	4.6 ± 0.1	4.6 ± 0.1	4.7 ± 0.2	4.6 ± 0.2
Endocortical Perimeter (mm)	3.5 ± 0.1	3.5 ± 0.2	3.3 ± 0.1	3.4 ± 0.1	3.5 ± 0.2	3.5 ± 0.2
Density of Material (mg HA/cm^3)	1025 ± 5.4	1014 ± 17.6	1208 ± 8	1214 ± 21	1199 ± 16	1192 ± 22

Females	**1 Month**		**3 Month**		**6 Month**	
	Control n = 6	***Nfatc1*$^{\Delta/\Delta}$ n = 3**	**Control n = 5**	***Nfatc1*$^{\Delta/\Delta}$ n = 4**	**Control n = 6**	***Nfatc1*$^{\Delta/\Delta}$ n = 6**
Distal Femur Trabecular Bone						
Bone Volume/Total Volume (%)	6.3 ± 1.4	5.5 ± 2.3	1.5 ± 0.4	1.4 ± 0.6	0.9 ± 0.4	0.8 ± 0.2
Trabecular Separation (μm)	176 ± 18	193 ± 53	335 ± 20	345 ± 15	444 ± 57	465 ± 52
Trabecular Number (1/mm)	5.7 ± 0.5	5.5 ± 1.4	3.0 ± 0.2	2.9 ± 0.1	2.3 ± 0.3	2.2 ± 0.2
Trabecular Thickness (μm)	21 ± 1	20 ± 1	30 ± 4	29 ± 4	32 ± 6	34 ± 5
Connectivity Density (1/mm^3)	367 ± 111	243 ± 250	12 ± 8	19 ± 15	13 ± 12	10 ± 5
Structure Model Index	3.1 ± 0.2	3.2 ± 0.2	3.7 ± 0.2	3.6 ± 0.3	3.7 ± 0.6	3.6 ± 0.1
Density of Material (mg HA/cm^3)	892 ± 14	899 ± 19	995 ± 15	996 ± 20	1039 ± 29	1050 ± 125
	n = 5	**n = 3**	**n = 5**	**n = 3**	**n = 5**	**n = 6**
Bone Volume/Total Volume (%)	81.9 ± 1.6	82.2 ± 2.0	87.9 ± 0.7	87.2 ± 0.9	90.0 ± 0.8	90.2 ± 0.8
Porosity (%)	18.1 ± 1.6	17.8 ± 2.0	12.1 ± 0.7	128 ± 0.9	10.0 ± 0.8	9.8 ± 0.8
Cortical Thickness (μm)	82 ± 9	85 ± 11	156 ± 9	147 ± 10	180 ± 4	175 ± 5

Females	**1 Month**		**3 Month**		**6 Month**	
	Control n = 6	***Nfatc1*$^{\Delta/\Delta}$ n = 3**	**Control n = 5**	***Nfatc1*$^{\Delta/\Delta}$ n = 4**	**Control n = 6**	***Nfatc1*$^{\Delta/\Delta}$ n = 6**
Total Area (mm^2)	1.4 ± 0.2	1.4 ± 0.1	1.7 ± 0.1	1.7 ± 0.1	1.6 ± 0.1	1.7 ± 0.1
Bone Area (mm^2)	0.4 ± 0.1	0.4 ± 0.1	0.8 ± 0.11	0.8 ± 0.1	0.8 ± 0.1	0.8 ± 0.1
Periosteal Perimeter (mm)	4.2 ± 0.3	4.1 ± 0.2	4.6 ± 0.1	4.6 ± 0.1	4.5 ± 0.2	4.6 ± 0.1
Endocortical Perimeter (mm)	3.5 ± 0.2	3.4 ± 0.1	3.3 ± 0.1	3.4 ± 0.1	3.2 ± 0.1	3.3 ± 0.1
Density of Material (mg HA/cm^3)	1007 ± 16	1022 ± 14	1217 ± 14	1221 ± 23	1225 ± 14	1219 ± 21

µCT was performed in distal femurs for trabecular bone and midshaft for cortical bone from 1, 3 and 6 month old male and female *BGLAP-Cre;Nfatc1*$^{\Delta/\Delta}$ mice and sex-matched control littermates. Values are means ± SD.

Table 5.

Femoral microarchitecture assessed by μCT of 1 and 4 month old *BGLAP-Cre;Nfatc2*$^{\Delta/\Delta}$ male and female mice and sex-matched *Nfatc2*$^{loxP/loxP}$ littermate controls.

Males	**1 Month**		**4 Month**	
	Control n = 6	***Nfatc2*$^{\Delta/\Delta}$ n = 5**	**Control n = 7**	***Nfatc2*$^{\Delta/\Delta}$ n = 6**
Distal Femur Trabecular Bone				
Bone Volume/Total Volume (%)	4.3 ± 0.9	4.5 ± 0.8	10.1 ± 3.4	9.4 ± 4.3
Trabecular Separation (μm)	239 ± 25	234 ± 17	223 ± 15	226 ± 12
Trabecular Number (1/mm)	4.2 ± 0.4	4.3 ± 0.3	4.5 ± 0.3	4.4 ± 0.2
Trabecular Thickness (μm)	24 ± 1	23 ± 1	40 ± 3	38 ± 7
Connectivity Density (1/mm^3)	170 ± 86	174 ± 97	198 ± 57	198 ± 47
Structure Model Index	3.1 ± 0.2	3.1 ± 0.2	2.2 ± 0.5	2.3 ± 0.5
Density of Material (mg HA/cm^3)	811 ± 5	806 ± 11	959 ± 26	971 ± 28
Femoral Midshaft Cortical Bone				
Bone Volume/Total Volume (%)	81.6 ± 0.8	81.4 ± 1.0	89.2 ± 0.8	89.5 ± 0.2
Porosity (%)	18.4 ± 0.8	18.6 ± 1.0	10.8 ± 0.8	10.5 ± 0.2
Cortical Thickness (μm)	85 ± 4	87 ± 4	167 ± 1	168 ± 6
Total Area (mm^2)	1.4 ± 0.1	1.6 ± 0.1	1.9 ± 0.2	1.9 ± 0.1
Bone Area (mm^2)	0.4 ± 0.1	0.5 ± 0.1	0.9 ± 0.1	0.9 ± 0.1
Periosteal Perimeter (mm)	4.2 ± 0.2	4.4 ± 0.2	4.9 ± 0.3	4.8 ± 0.2
Endocortical Perimeter (mm)	3.5 ± 0.2	3.7 ± 0.1	3.6 ± 0.3	3.5 ± 0.2
Density of Material (mg HA/cm^3)	811 ± 5	806 ± 11	1218 ± 20	1217 ± 14

Females	**1 Month**		**4 Month**	
	Control n = 6	***Nfatc2*$^{\Delta/\Delta}$ n = 6**	**Control n = 7**	***Nfatc2*$^{\Delta/\Delta}$ n = 7**
Distal Femur Trabecular Bone				
Bone Volume/Total Volume (%)	3.8 ± 0.7	3.8 ± 0.6	4.7 ± 1.0	5.5 ± 0.8
Trabecular Separation (μm)	254 ± 53	250 ± 25	305 ± 11	296 ± 29
Trabecular Number (1/mm)	4.1 ± 0.7	4.1 ± 0.4	3.3 ± 0.1	3.4 ± 0.3
Trabecular Thickness (μm)	23 ± 1	23 ± 1	39 ± 3	41 ± 2
Connectivity Density (1/mm^3)	149 ± 49	120 ± 32	108 ± 34	112 ± 31
Structure Model Index	3.1 ± 0.1	3.1 ± 0.2	3.0 ± 0.3	2.7 ± 0.2
Density of Material (mg HA/cm^3)	804 ± 5	807 ± 3	1017 ± 28	997 ± 41
Femoral Midshaft Cortical Bone				
Bone Volume/Total Volume (%)	80.4 ± 2.3	82.6 ± 0.9	89.4 ± 0.6	89.0 ± 1.5
Porosity (%)	19.6 ± 2.3	17.4 ± 0.9	10.6 ± 0.6	11.0 ± 1.5
Cortical Thickness (μm)	81 ± 7	90 ± 0.3 *	174 ± 4	178 ± 11
Total Area (mm^2)	1.4 ± 0.2	1.4 ± 0.2	1.6 ± 0.1	1.6 ± 0.1

Females	**1 Month**		**4 Month**	
	Control n = 6	***Nfatc2*$^{\Delta/\Delta}$ n = 6**	**Control n = 7**	***Nfatc2*$^{\Delta/\Delta}$ n = 7**
Bone Area (mm^2)	0.4 ± 0.1	0.5 ± 0.1	0.8 ± 0.1	0.8 ± 0.1
Periosteal Perimeter (mm)	4.1 ± 0.3	4.2 ± 0.3	4.5 ± 0.1	4.5 ± 0.1
Endocortical Perimeter (mm)	3.4 ± 0.2	3.5 ± 0.3	3.2 ± 0.1	3.2 ± 0.2
Density of Material (mg HA/cm^3)	985 ± 19	998 ± 7	1250 ± 30	1254 ± 24

µCT was performed in distal femurs for trabecular bone and midshaft for cortical bone from 1 and 4 month old male and female *BGLAP-Cre;Nfatc2*$^{\Delta/\Delta}$ mice and sex-matched control littermates. Values are means ± SD.

*Significantly different between control and *BGLAP-Cre;Nfatc2*$^{\Delta/\Delta}$, $p < 0.05$ by unpaired *t*-test.

Table 6.

Femoral microarchitecture assessed by μCT of 1 and 4 month old *BGLAP-Cre; Nfatc1$^{\Delta/\Delta}$;Nfatc2$^{\Delta/\Delta}$* male and female mice and sex-matched *Nfatc1$^{loxP/loxP}$;Nfatc2$^{loxP/loxP}$* littermate controls.

Males	**1 Month**		**4 Month**	
	Control n = 6	***Nfatc1$^{\Delta/\Delta}$;c2$^{\Delta/\Delta}$* n = 6**	**Control n = 3**	***Nfatc1$^{\Delta/\Delta}$;c2$^{\Delta/\Delta}$* n = 8**
Distal Femur Trabecular Bone				
Bone Volume/Total Volume (%)	7.4 ± 3.9	7.0 ± 3.2	10.4 ± 4.0	7.5 ± 1.5
Trabecular Separation (μm)	216 ± 22	221 ± 15	217 ± 17	235 ± 14
Trabecular Number (1/mm)	4.7 ± 0.4	4.6 ± 0.3	4.6 ± 0.3	4.2 ± 0.2
Trabecular Thickness (μm)	20 ± 1	20 ± 3	38 ± 5	36 ± 3
Connectivity Density (1/mm^3)	166 ± 89	129 ± 88	211 ± 67	149 ± 36
Structure Model Index	3.2 ± 0.3	3.3 ± 0.2	2.0 ± 0.6	2.4 ± 0.3
Density of Material (mg HA/cm^3)	892 ± 41	903 ± 41	938 ± 8	943 ± 10
Femoral Midshaft Cortical Bone				
Bone Volume/Total Volume (%)	83.5 ± 1.5	84.6 ± 1.2	89.8 ± 0.3	89.4 ± 0.5
Porosity (%)	16.5 ± 1.5	15.4 ± 1.2	10.2 ± 0.3	10.6 ± 0.5
Cortical Thickness (μm)	77 ± 7	78 ± 5	174 ± 4	166 ± 7
Total Area (mm^2)	1.3 ± 0.1	1.3 ± 0.2	1.7 ± 0.1	1.9 ± 0.3
Bone Area (mm^2)	0.4 ± 0.1	0.4 ± 0.1	0.8 ± 0.1	0.9 ± 0.1
Periosteal Perimeter (mm)	4.0 ± 0.2	4.1 ± 0.3	4.6 ± 0.2	4.9 ± 0.3
Endocortical Perimeter (mm)	3.4 ± 0.2	3.5 ± 0.2	3.3 ± 0.2	3.6 ± 0.3
Density of Material (mg HA/cm^3)	926 ± 22	951 ± 25	1251 ± 14	1235 ± 16

Females	**1 Month**		**4 Month**	
	Control n = 5	***Nfatc1$^{\Delta/\Delta}$;c2$^{\Delta/\Delta}$* n = 6**	**Control n = 6**	***Nfatc1$^{\Delta/\Delta}$;c2$^{\Delta/\Delta}$* n = 6**
Distal Femur Trabecular Bone				
Bone Volume/Total Volume (%)	4.1 ± 1.8	3.8 ± 0.9	4.4 ± 1.2	3.6 ± 0.2
Trabecular Separation (μm)	203 ± 26	223 ± 35	294 ± 23	320 ± 32
Trabecular Number (1/mm)	5.0 ± 0.7	4.6 ± 0.7	3.4 ± 0.2	3.2 ± 0.1
Trabecular Thickness (μm)	19 ± 2	20 ± 1	34 ± 3	37 ± 3
Connectivity Density (1/mm^3)	193 ± 161	168 ± 59	87 ± 27	46 ± 11 *
Structure Model Index	3.2 ± 0.2	3.2 ± 0.2	2.8 ± 0.2	3.0 ± 0.2 *
Density of Material (mg HA/cm^3)	883 ± 15	884 ± 8	920 ± 28	952 ± 19 *
Femoral Midshaft Cortical Bone				
Bone Volume/Total Volume (%)	82.8 ± 3.9	84.6 ± 0.9	90.0 ± 0.2	89.9 ± 0.3
Porosity (%)	17.2 ± 3.9	15.4 ± 0.9	10.0 ± 0.2	10.1 ± 0.3
Cortical Thickness (μm)	74 ± 12	78 ± 3	175 ± 5	173 ± 6
Total Area (mm^2)	1.3 ± 0.2	1.4 ± 0.2	1.5 ± 0.1	1.6 ± 0.1

Females	**1 Month**		**4 Month**	
	Control n = 5	***Nfatc1*$^{\Delta/\Delta}$;*c2*$^{\Delta/\Delta}$ n = 6**	**Control n = 6**	***Nfatc1*$^{\Delta/\Delta}$;*c2*$^{\Delta/\Delta}$ n = 6**
Bone Area (mm^2)	0.4 ± 0.1	0.4 ± 0.1	0.8 ± 0.1	0.8 ± 0.1
Periosteal Perimeter (mm)	4.1 ± 0.3	4.2 ± 0.3	4.4 ± 0.1	4.5 ± 0.1
Endocortical Perimeter (mm)	3.5 ± 0.3	3.6 ± 0.3	3.1 ± 0.1	3.2 ± 0.1
Density of Material (mg HA/cm^3)	941 ± 37	948 ± 22	1269 ± 7	1268 ± 13

µCT was performed in distal femurs for trabecular bone and midshaft for cortical bone from 1 and 4 month old male and female *BGLAP-Cre;Nfatc1*$^{\Delta/\Delta}$*;Nfatc2*$^{\Delta/\Delta}$ mutant mice and sex-matched control littermates. Values are means ± SD.

*Significantly different between control and *BGLAP-Cre;Nfatc1*$^{\Delta/\Delta}$*;Nfatc2*$^{\Delta/\Delta}$, $p < 0.05$ by unpaired *t*-test.